Deformation and spin-orbit splitting of Λ hypernuclei in the Skyrme-Hartree-Fock approach

Huai-Tong Xue (薛怀通),[1] Yi-Fan Chen (陈伊凡),[1] Q. B. Chen (陈启博),[1] Y. A. Luo (罗延安),[2] H.-J. Schulze,[3] and Xian-Rong Zhou (周先荣)[1,*]

[1]*Department of Physics, East China Normal University, Shanghai 200241, China*

[2]*School of Physics, Nankai University, Tianjin 300071, China*

[3]*INFN Sezione di Catania, Dipartimento di Fisica, Universitá di Catania, Via Santa Sofia 64, 95123 Catania, Italy*

(Received 10 March 2023; accepted 5 April 2023; published 25 April 2023)

The realizations of spin symmetry in the Λ hyperon spectra of hypernuclei ranging from light to heavy masses are investigated in the framework of the deformed Skyrme-Hartree-Fock approach. The effect of deformation on spin symmetry and its interplay with the required spin-orbit force is studied in detail. It is found that the spin symmetry prevails due to a small spin-orbit force. Moreover, for spin doublets with the same principal quantum number n, the reduced spin-orbit splitting $\Delta E_{\text{s.o.}}$ shows a good linear relation with respect to the quantum number l, even for a large ΛN spin-orbit strength.

DOI: 10.1103/PhysRevC.107.044317

I. INTRODUCTION

Spin symmetry (SS) in the single-particle (s.p.) levels of atomic nuclei, i.e., the quasidegeneracy between two s.p. states with quantum numbers $(n, l, j = l - 1/2)$ and $(n, l, j = l + 1/2)$, is of great importance to nuclear structure and has been extensively discussed in the literature for nucleons and antinucleons [1–4]. In ordinary nuclei, the s.p. spectra are characterized by an obvious violation of SS. This spin-orbit (s.o.) splitting of the spin doublets $(n, l, j = l \pm 1/2)$ caused by the s.o. interaction, lays the foundation for explaining the traditional magic numbers in nuclear physics [1,2]. The SS was also studied in antinucleon spectra [5,6]. There is a relativistic origin for SS in the antinucleon spectra, while SS is much more conserved in real nuclei [5].

Splittings of spin doublets combined with those of pseudospin doublets play critical roles in the evolution of magic numbers in exotic nuclei [4], discovered by modern spectroscopic studies with radioactive ion beam facilities, and thus further affect the microstructure and other properties of atomic nuclei. They can account for various nuclear structure features, e.g., deformation [7], superdeformation [8], magnetic moment [9], and identical rotational bands [10].

The study of SS in hyperonic s.p. levels of hypernuclei is also an interesting topic that may help us further understand the hypernuclear structure and hyperon-nucleon interaction. In hypernuclei, hyperons together with neutrons and protons jointly influence the structure of this quantum system. Since the discovery of the first hyperfragment in an emulsion exposed to cosmic rays in 1953 [11], hypernuclei have been investigated extensively both theoretically and experimentally to understand the hyperon-nucleon and hyperon-hyperon interactions, which is crucial not only for hypernuclear structure [12], but also for neutron stars [13–18].

In contrast to nuclear systems, the s.o. splitting of Λ states in hypernuclei is much smaller [19–21], because the strange quark contributes little to the nuclear force. In detail, the observed s.o. splitting of the $1p$ state in the hypernucleus ${}^{13}_{\Lambda}\text{C}$ is only $\Delta E_{\text{s.o.}} = 0.152 \pm 0.090$ MeV [20], which is 20–30 times smaller than that in ordinary nuclei. Moreover, the s.o. splitting of the $1f$ state in the hypernucleus ${}^{89}_{\Lambda}\text{Y}$ is very small as well, namely $E(1f_{5/2}) - E(1f_{7/2}) = 0.2 \pm 0.06$ MeV [21]. To model such small s.o. splitting, the ΛN s.o. force and tensor coupling were introduced to the Skyrme-Hartree-Fock (SHF) [22–24] and relativistic-mean-field (RMF) [25,26] approaches. The SHF studies reasonably reproduce the s.o. splitting of Λ $1p$ states in ${}^{13}_{\Lambda}\text{C}$ with a small s.o. coupling strength [23,24]. Within the relativistic Hartree-Fock theory, and adjusting the meson-hyperon coupling strength [27], the Λ $1p$ splitting in ${}^{16}_{\Lambda}\text{O}$ is obtained around the empirical value $\Delta E_{\text{s.o.}} = 0.3$–$0.6$ MeV [28]. Small spin-orbit splittings of hyperon s.p. levels in ${}^{208}_{\Lambda}\text{Pb}$ were also predicted within RMF [29].

To describe hypernuclear properties adequately, several types of phenomenological and more microscopic ΛN interactions have been proposed, like the Skyrme [22,30–37], the Nijmegen soft-core [38–41], the Nijmegen extended-soft-core [42–47], relativistic [48–55], as well as chiral interactions [56–58]. They have been employed in appropriate theoretical approaches, such as the shell model [59,60], cluster model [61,62], antisymmetrized molecular dynamics model [63–68], nonrelativistic and relativistic mean-field model [24,41,52–55,69–79], and the beyond-mean-field approach [23,80–84]. In particular, the SHF formalism has been used for the description of phenomena like removal energies [22,77,85], deformation [41,78,86], hyperon halos [24,87], and pairing correlations [79].

In this paper we will extend the SHF approach to perform a systematic theoretical study of hyperon SS in deformed nuclei. Considering that the deformation of a hypernucleus can also lead to the splitting of hyperon s.p. levels, it is necessary to study the dependence of the ΛN s.o. interaction

*xrzhou@phy.ecnu.edu.cn

on deformation in these cases. This can help to improve the modeling of the ΛN interaction by including deformation in the future. We will use the deformed SHF (DSHF) theory [88] and employ the Skyrme force SLy4 [89] for the NN interaction in combination with the SLL4 [22,37] ΛN Skyrme interaction, which is optimized for fitting the complete current data set of single-Λ hypernuclei in spherical SHF calculations [37,77]. We will first study the impact of deformation on the effectiveness of these interactions to describe the Λ removal energies of different orbitals, and then introduce a ΛN s.o. force to investigate its dependence on deformation. Finally, the SS of the large hypernucleus ${}^{208}_{\Lambda}$Pb will be examined in detail.

The paper is organized as follows. In Sec. II, the theoretical DSHF approach for hypernuclei is briefly introduced. In Sec. III, the Λ removal energies, the density distributions of the hypernuclei and the Λ hyperon, the combined effects of deformation and the s.o. interaction, and the SS in the hyperon spectrum of ${}^{208}_{\Lambda}$Pb are discussed in detail. Finally, a summary is given in Sec. IV.

II. THEORETICAL FRAMEWORK

In the DSHF approach, the total energy of a hypernucleus is given by [31,41,71,85,86,88]

$$E = \int d^3\boldsymbol{r}\, \varepsilon(\boldsymbol{r})\,, \tag{1}$$

where the energy-density functional is

$$\varepsilon = \varepsilon_N[\rho_n, \rho_p, \tau_n, \tau_p, \boldsymbol{J}_n, \boldsymbol{J}_p] + \varepsilon_\Lambda[\rho_n, \rho_p, \rho_\Lambda, \tau_\Lambda, \boldsymbol{J}_N, \boldsymbol{J}_\Lambda] \tag{2}$$

with ε_N and ε_Λ as contributions from NN and ΛN interactions, respectively. For the nucleonic functional ε_N, we use the standard Skyrme force SLy4 [89]. The one-body density ρ_q, kinetic density τ_q, and s.o. current $\boldsymbol{J}_q$ read

$$[\rho_q,\ \tau_q,\ \boldsymbol{J}_q] = \sum_{k=1}^{N_q} n_q^k \left[|\phi_q^k|^2,\ |\nabla\phi_q^k|^2,\ \phi_q^{k*}(\nabla\phi_q^k \times \boldsymbol{\sigma})/i\right], \tag{3}$$

where ϕ_q^k $(k = 1, \ldots, N_q)$ are the s.p. wave functions of the kth occupied states for the different particles $q = n, p, \Lambda$. The occupation probabilities n_q^k are calculated by taking into account pairing within a Bardeen–Cooper–Schrieffer (BCS) approximation for nucleons only. The pairing interaction between nucleons is taken as a density-dependent δ force [90,91],

$$V_q(\boldsymbol{r}_1, \boldsymbol{r}_2) = V_q'\left[1 - \frac{\rho_N((\boldsymbol{r}_1+\boldsymbol{r}_2)/2)}{0.16\,\mathrm{fm}^{-3}}\right]\delta(\boldsymbol{r}_1 - \boldsymbol{r}_2)\,, \tag{4}$$

where pairing strengths $V_p' = V_n' = -410$ MeV fm^3 are used for light nuclei [92], while $V_p' = -1146$ MeV fm^3, $V_n' = -999$ MeV fm^3 for medium-mass and heavy nuclei [41]. A smooth energy cutoff is employed in the BCS calculations [93]. In the case of an odd nucleon number the orbit occupied by the unpaired nucleon is blocked as described in Ref. [94].

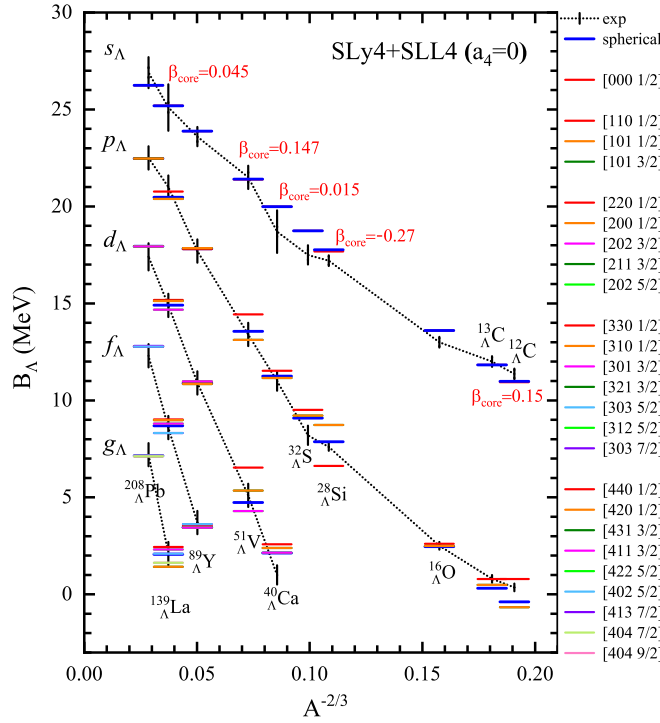

FIG. 1. The removal energies of the major Λ s.p. shells in several hypernuclei obtained with the original SLy4 NN and SLL4 ΛN Skyrme-type interactions, without (horizontal blue bars) and with (other colors) considering deformation, in comparison with experimental data [96] (vertical black bars). The spherical results are obtained by mixing several deformed orbits with the same occupation probability. The predicted core deformation, Eq. (8), is indicated for the relevant hypernuclei.

Through the variation of the total energy Eq. (1) one derives the SHF Schrödinger equation for both nucleons and hyperons,

$$\left[-\nabla\cdot\frac{1}{2m_q^*(\boldsymbol{r})}\nabla + V_q(\boldsymbol{r}) - i\boldsymbol{W}_q(\boldsymbol{r})\cdot(\nabla\times\boldsymbol{\sigma})\right]\phi_q^k(\boldsymbol{r}) = e_q^k\phi_q^k(\boldsymbol{r})\,, \tag{5}$$

where $V_q(\boldsymbol{r})$ is the central part of the mean field depending on the densities, while $\boldsymbol{W}_q(\boldsymbol{r})$ is the s.o. interaction part [88,90].

For the Skyrme-type interactions, ε_Λ is given as [22,31,33,35,37]

$$\begin{aligned}\varepsilon_\Lambda =& \frac{\tau_\Lambda}{2m_\Lambda} + a_0\rho_\Lambda\rho_N + a_3\rho_\Lambda\rho_N^{1+\alpha} + a_3'\rho_\Lambda\left(\rho_N^2 + 2\rho_n\rho_p\right)\\ &+ a_1(\rho_\Lambda\tau_N + \rho_N\tau_\Lambda) - a_2(\rho_\Lambda\Delta\rho_N + \rho_N\Delta\rho_\Lambda)/2\\ &- a_4(\rho_\Lambda\nabla\cdot\boldsymbol{J}_N + \rho_N\nabla\cdot\boldsymbol{J}_\Lambda)\,,\end{aligned} \tag{6}$$

where the last term is the s.o. part, which is adjusted to reproduce the observed s.o. splitting of ${}^{13}_{\Lambda}$C in our approach [24,87,95]. Two alternative parametrizations of nonlinear effects are indicated, i.e., the first one a_3 derived from a G matrix [32,36,69] and the second one a_3' from a ΛNN contact force [30,31]. The SLL4 ΛN force used in this work employs the first choice. For convenience we repeat here the parameters [37]: $\alpha = 1$, $a_{0,1,2,3} = [-322.0, 15.75, 19.63, 715.0]$ (in ap-

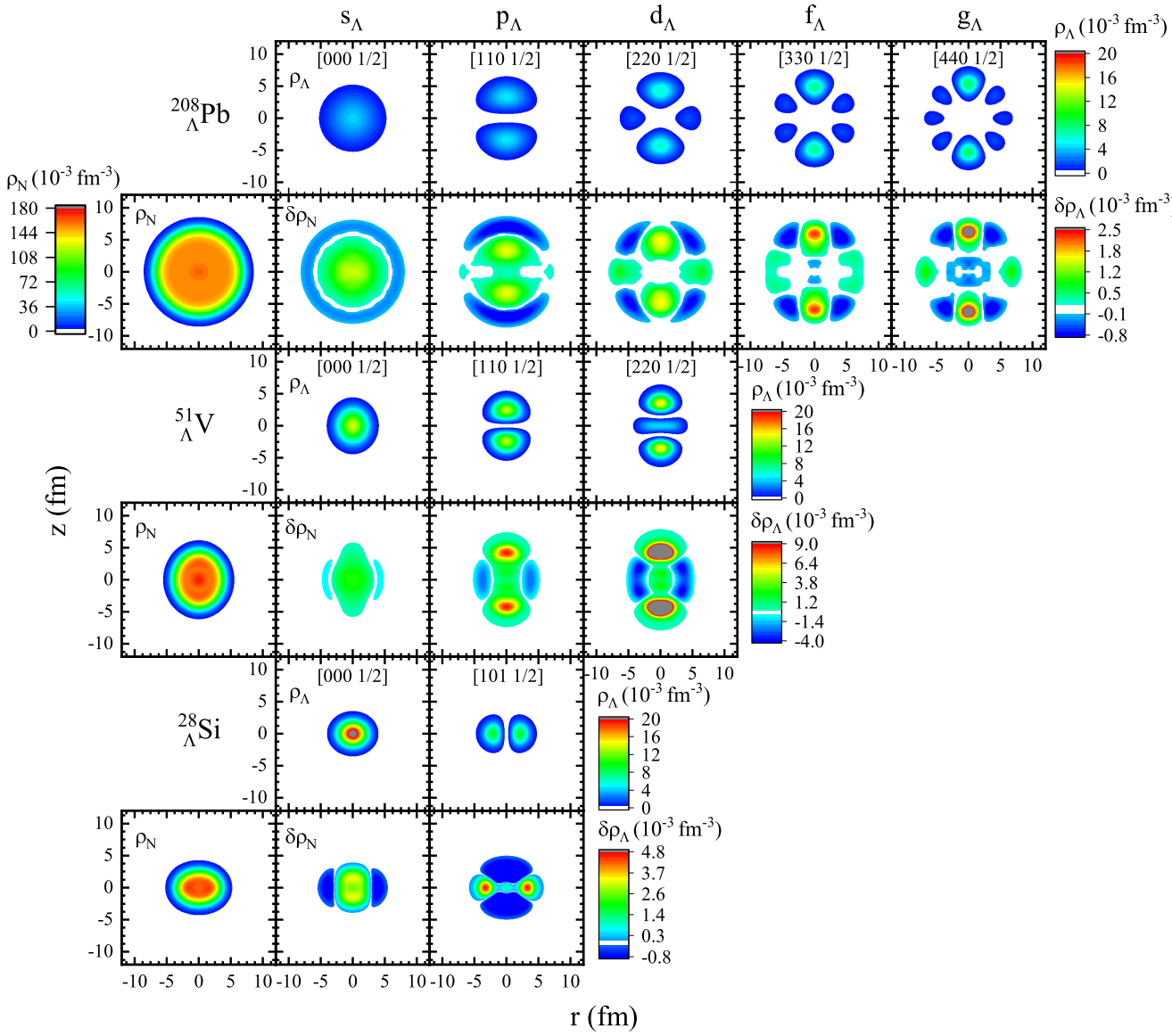

FIG. 2. Two-dimensional density distributions ρ_Λ of different Λ orbits and the change of nucleonic background density $\delta\rho_N$, Eq. (10), in the (r, z) plane, for $^{208}_{\Lambda}$Pb, $^{51}_{\Lambda}$V, and $^{28}_{\Lambda}$Si, obtained with the SLy4 + SLL4 interaction. The leftmost panels show the density of the core nuclei.

propriate units for ρ given in fm^{-3} and ε in MeV fm^{-3}), whereas a_4 will be discussed later.

In the present calculations, the DSHF Schrödinger equation is solved in cylindrical coordinates (r, z), under the assumption of axial symmetry of the mean fields. The optimal quadrupole deformation parameters

$$\beta_2^{(q)} = \sqrt{\frac{\pi}{5}}\frac{\langle 2z^2 - r^2\rangle_q}{\langle z^2 + r^2\rangle_q} \tag{7}$$

are calculated by minimizing the energy density functional. However, when comparing with experimental deformations derived from the quadrupole moment Q_p, we employ the definition

$$\beta = \frac{\sqrt{5\pi}}{3}\frac{Q_p}{ZR_0^2} \tag{8}$$

with $R_0 \equiv 1.2\,A^{1/3}$ fm [86,92,97,98,105].

III. RESULTS AND DISCUSSION

A. Removal energies

The experimental Λ removal energies

$$B_\Lambda = E\left({}^{A}_{\Lambda}Z\right) - E\left({}^{A-1}Z\right) \tag{9}$$

in the different Λ shells are quite close to the corresponding Λ s.p. energies due to the absence of the Pauli exclusion principle and the small core rearrangement effects of the single Λ hyperon. Therefore, these values will allow us to analyze the SS in the Λ hyperon spectrum.

To study the accuracy of the Skyrme-type interactions SLy4 + SLL4 to reproduce the removal energies, we calculate B_Λ of hypernuclei in the whole nuclear chart. Figure 1

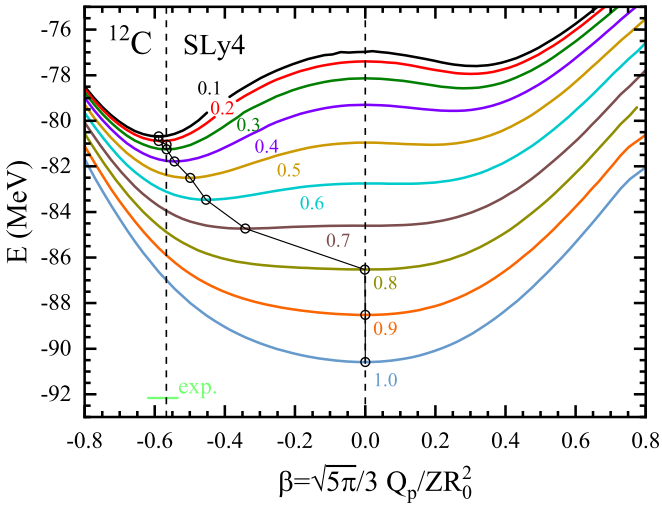

FIG. 3. Potential energy surfaces of ^{12}C obtained with different reduction factors γ of the SLy4 s.o. force (indicated near the curves). The markers indicate the minima of each curve, in comparison with the experimental value [97,98].

shows the results with and without considering deformation. One should stress that the Skyrme parameters of all current ΛN Skyrme forces have been determined in spherical calculations, and thus in principle should be refitted by allowing deformation, which we will not attempt in this work, but rather use the standard forces. Doing so, some nuclear cores are predicted as deformed by the SLy4 force, with the values of the deformation β indicated in the plot. Comparing the removal energies of undeformed (horizontal blue bars) and deformed (other colors) calculations in these cases, one notes that the difference for the Λ 1s states is very small, whereas the higher s.p. states split up according to the magnitude of deformation, which will be analyzed in more detail later. Of those states, usually the most bound one is expected to be physically realized. As the level splittings are of the order of 1 MeV, this demonstrates that high-precision hypernuclear spectroscopy will also require precise theoretical modeling, including in particular the core deformation. Vice versa, precise experimental results for higher Λ s.p. levels [106] could provide indications on the core deformation.

B. Density distributions

In Fig. 2 we illustrate the impurity effects caused by the inclusion of the Λ hyperon for the three hypernuclei $^{208}_{\Lambda}$Pb, $^{51}_{\Lambda}$V, and $^{28}_{\Lambda}$Si, of which the first is spherical, the second prolate, and the third oblately deformed, with the deformation β given in Fig. 1. The odd rows show the two-dimensional Λ density distributions with the Λ occupying different major shells, and the even rows the density change of the nuclear core, e.g.,

$$\delta\rho_N \equiv \rho_N\left[^{208}_{\Lambda}\mathrm{Pb}\right] - \rho_N[^{207}\mathrm{Pb}]\,. \tag{10}$$

The density profiles of the core nuclei are shown in the leftmost column.

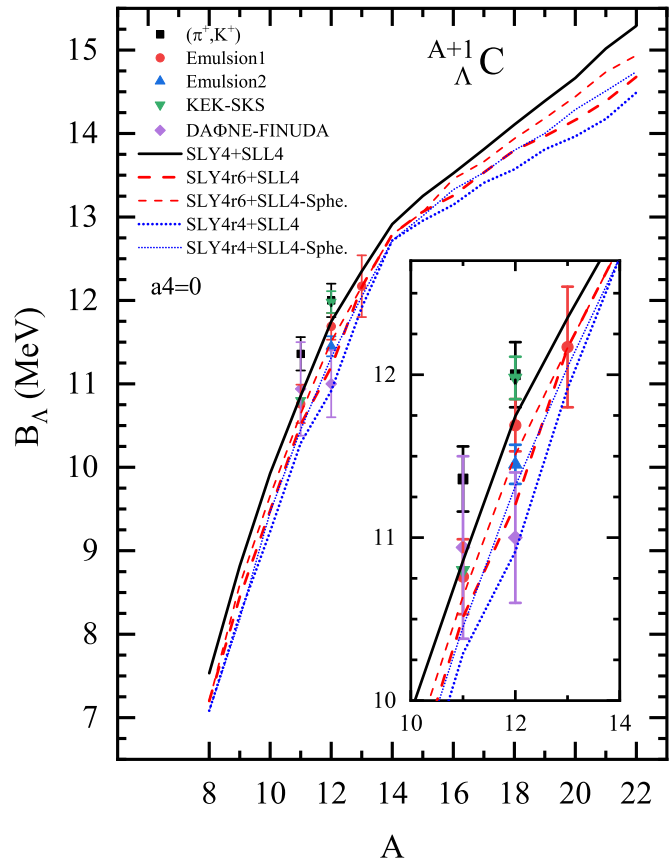

FIG. 4. Λ 1s removal energies of hypernuclei $^{A+1}_{\Lambda}$C obtained with SLy4 (the original interaction), SLy4r6 (s.o. reduction factor $\gamma = 0.6$), SLy4r4 ($\gamma = 0.4$) NN, and the SLL4($a_4 = 0$) ΛN interaction, in undeformed (thin curves) and deformed (thick curves) calculations. The experimental data (π^+, K^+) [96,99], Emulsion1 [100], Emulsion2 [101], KEK-SKS [102], and DAΦNE-FINUDA [103,104] are also shown.

The shapes of the hyperon density distributions, including the symmetry properties and the numbers of nodes and peaks, are mainly determined by the spherical harmonics functions $Y_{lm}(\theta, \phi)$. In $\delta\rho_N$ one can clearly see the imprint of the Λ on the nucleonic background by the ΛN interaction: For the s_Λ orbitals one observes the shrinkage phenomenon of the nuclear core due to the attractive ΛN interaction [33,86,107–109]. For the p_Λ orbitals instead, the core deformation could be enhanced due to the large deformation of the nondegenerate Λ 1p states [24,110]. For heavy hypernuclei like $^{208}_{\Lambda}$Pb, the effect of the hyperon is fairly small, but more substantial for the lighter nuclei.

C. Effect of deformation on spin symmetry

To investigate the effect of deformation on spin symmetry, we first study $^{13}_{\Lambda}$C, for which the experimental s.o. splitting value of the Λ $1p_{1/2}$ and $1p_{3/2}$ states is known, $E(1/2^-) - E(3/2^-) = 0.152 \pm 0.054(\mathrm{stat}) \pm 0.036(\mathrm{syst})$ MeV [20,111], and the excitation energies of the $1/2^-$ and $3/2^-$ states were determined as 10.98 and 10.83 MeV, respectively. However, while the deformation of the core nucleus

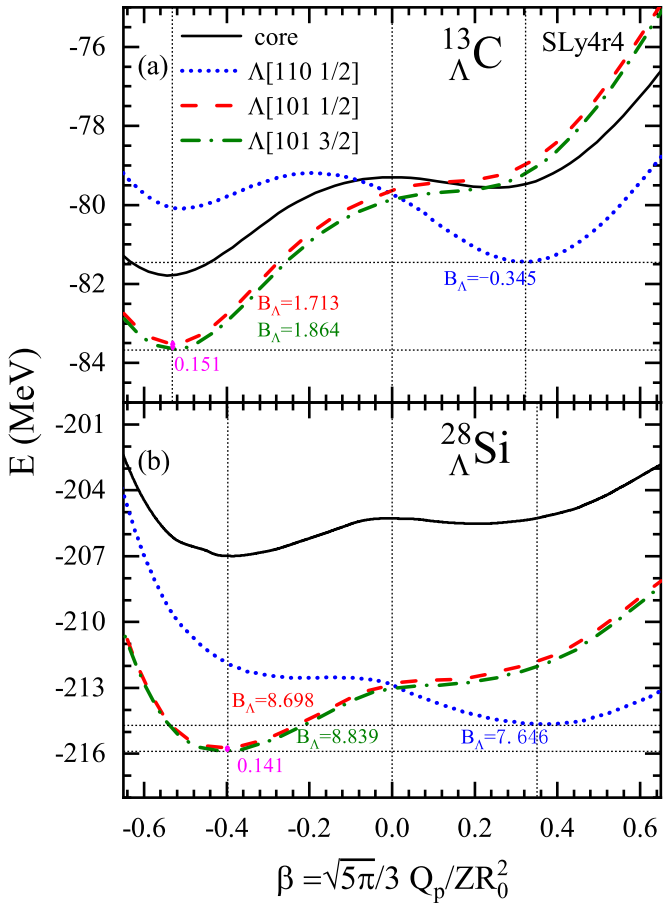

FIG. 5. Potential energy surfaces of different Λ $1p$ states for $^{13}_{\Lambda}$C, $^{28}_{\Lambda}$Si, and their core nuclei, obtained with SLy4r4 (s.o. reduction factor $\gamma = 0.4$)+SLL4(a_4=3.15 MeV fm^5) forces. B_Λ values are given in MeV.

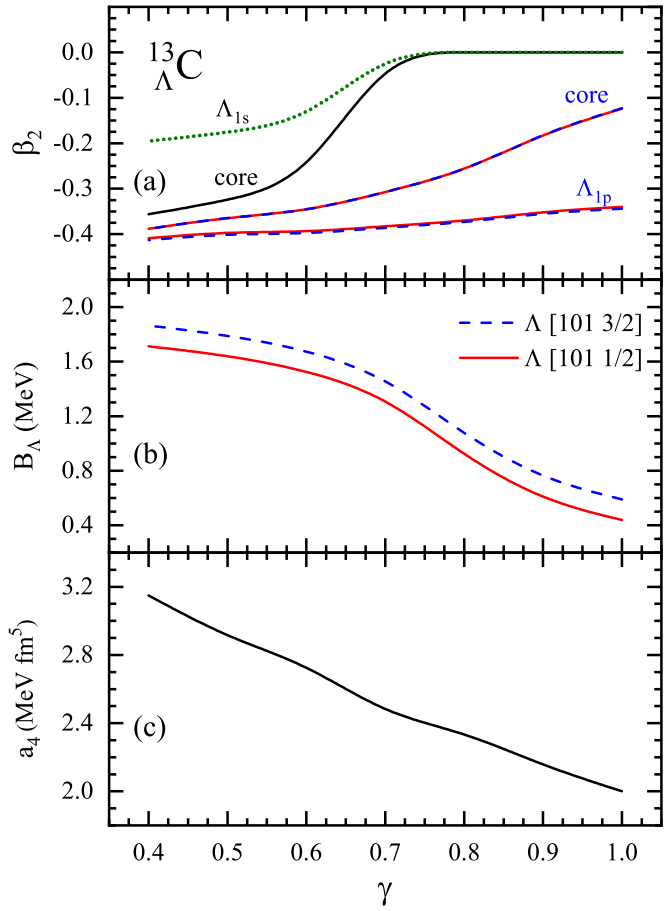

FIG. 6. Dependence of physical quantities for $^{13}_{\Lambda}$C on the NN s.o. reduction factor γ: (a) quadrupole deformations of core nucleus and Λ orbitals with occupied [101 (1,3)/2] $1p$ and [000 1/2] $1s$ states; (b) corresponding Λ removal energies; (c) ΛN s.o. force strength a_4 required to reproduce a 0.15 MeV $1p$ splitting.

^{12}C derived from its proton quadrupole moment Q_p is rather large, $\beta \approx -0.58 \pm 0.03$ [97,98], the NN interaction SLy4 predicts a spherical ground state [41,86,110,112]. In Ref. [112] it was pointed out that the s.o. splitting of the s.p. levels around the Fermi surface plays an essential role in driving the nuclear deformation. Therefore, empirically the NN s.o. interaction is reduced in order to obtain deformed minima [24,80,82,83,86,92,112,113], and we also follow this procedure to reproduce the proper β value.

The potential energy surfaces corresponding to different reduction factors γ of the SLy4 NN s.o. force are illustrated in Fig. 3. One observes that the theoretical quadrupole deformations are close to the experimental one for strong reductions $\gamma \lesssim 0.4$. This modification of the NN force also changes slightly the predictions for the Λ $1s$ removal energies of the carbon isotopes, which is illustrated in Fig. 4, where theoretical results obtained with $\gamma = 1, 0.6, 0.4$ in spherical and deformed calculations are compared. One observes that both the reduction of the NN s.o. force and the deformation of the core nucleus (which usually causes a smaller central nucleon density relevant for $1s$ states) slightly reduce the predicted B_Λ values, which remain however within the current experimental error bars. The appropriate procedure would be to refit the SLL4 ΛN force within the improved formalism by taking into account deformation, but we will not attempt that here, and rather focus on the ΛN s.o. force in the following, choosing a reduction value of $\gamma = 0.4$ for the NN s.o. force.

We then investigate the combined effect of deformation and ΛN s.o. force ($\sim a_4$) on the splitting of the Λ $1p$ states [110 1/2], [101 1/2], and [101 3/2] in $^{13}_{\Lambda}$C. Fig. 5(a) depicts the potential energy surfaces corresponding to these states. In the spherical calculation with $a_4 = 0$ all three states are degenerate and a small removal energy $B_{\Lambda_p} \approx 0.5$ MeV is predicted. However, since the core nucleus is strongly oblately deformed, the embedded oblate [101 1/2] and [101 3/2] states are energetically favored, and their binding rises to $B_{\Lambda_p} \approx 1.8$ MeV. On top of this, the small s.o. parameter $a_4 =$ 3.15 MeV fm^5 is fitted to reproduce the experimental s.o. splitting between the [101 1/2] and [101 3/2] states [24,87]. On the contrary, the prolate [110 1/2] state is energetically disfavored in the oblate ^{12}C core. It would be difficult to observe this state experimentally, as its excitation would require a collective configuration change from the oblate true ^{12}C ground state to the excited prolate one. The detailed modeling

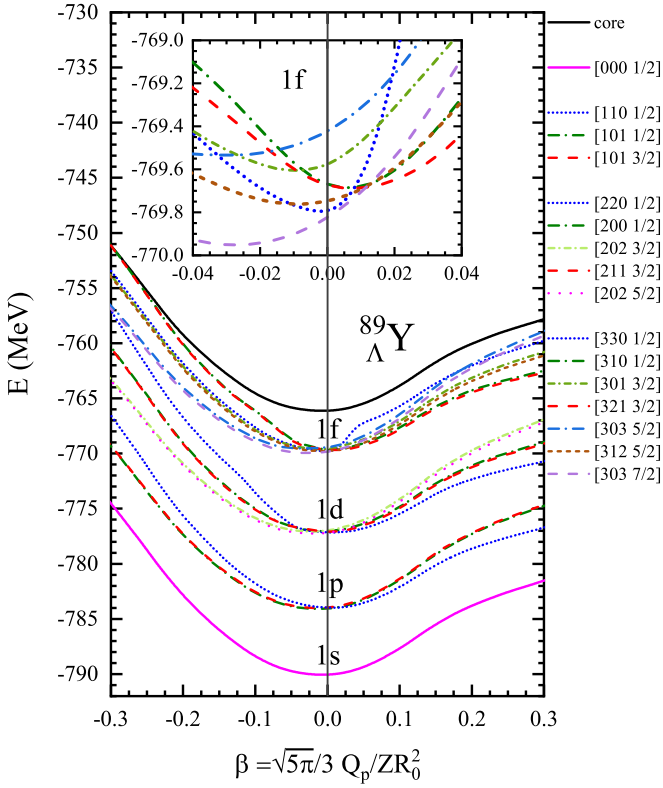

FIG. 7. Potential energy surfaces of $^{89}_{\Lambda}$Y with Λ occupying different states and of the core nucleus, obtained with SLy4($\gamma = 1$)+SLL4($a_4 = 3.15$ MeV fm^5) forces. The inset shows the $1f$ levels close to $\beta = 0$.

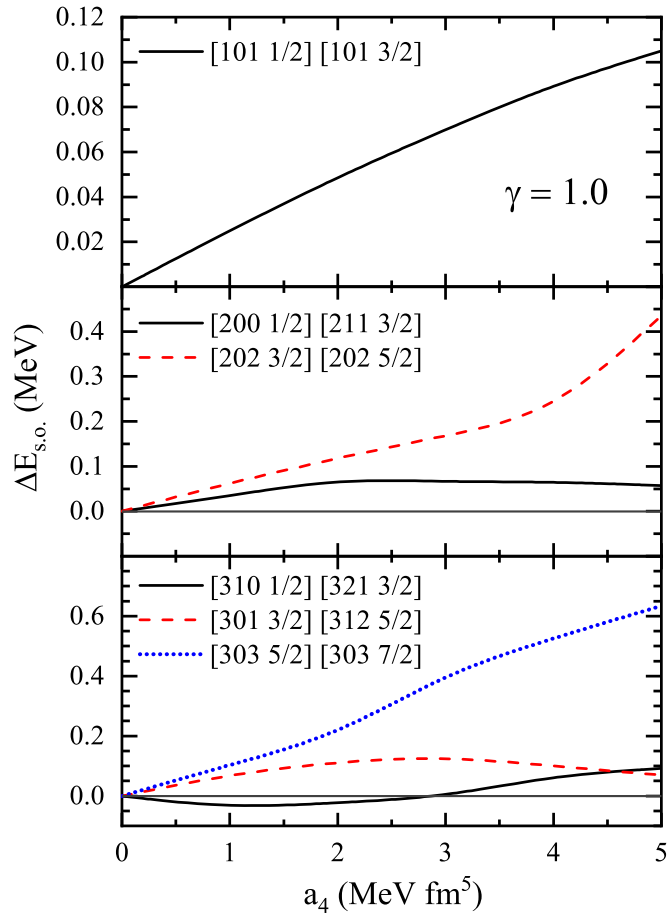

FIG. 8. Λ s.o. splittings of the $1p, d, f$ levels for $^{89}_{\Lambda}$Y as a function of a_4.

of this process would require a more sophisticated dynamical theoretical framework.

We note that the s.o. parameter $a_4 = 3.15$ MeV fm^5 is slightly larger than the one required in the spherical calculation for the same s.o. splitting, $a_4 = 2.35$ MeV fm^5 [87], which indicates clearly the interplay between deformation and s.o. force. This is examined in more detail in Fig. 6, which shows the dependence of $^{13}_{\Lambda}$C deformation properties on the s.o. reduction factor γ. Panel (a) shows the deformations of core nucleus and Λ density. Since the [101 1/2] and [101 3/2] Λ orbitals are both deformed, in this case also the nuclear core remains deformed even for $\gamma \approx 1$, where the pure ^{12}C nucleus and $^{13}_{\Lambda}$C with Λ $1s$ occupation are instead spherical (black and green curves), see also Fig. 3. One can clearly see the contraction or extension of the nuclear core due to the presence of a $1s$ or $1p$ Λ, respectively. The effect was illustrated in Fig. 2 (third column) for heavier nuclei. Figure 6(b) shows the change of B_Λ of both Λ $1p$ states with γ, in which their splitting is always constrained to 0.15 MeV. The binding increases with deformation due to the better overlap of Λ and nucleon densities indicated in panel (a). The predicted values for $\gamma = 0.4$ are about 1.8 MeV, close to experimental result of about 1.1 MeV [96]. As stated before, in the future deformation should be included in an improved global fitting procedure of the SLL4 force. The value of a_4 reproducing the 0.15 MeV splitting of the $1p$ doublet in $^{13}_{\Lambda}$C is shown in Fig. 6(c).

Coming back to Fig. 5, in panel (b) the s.o. splitting is studied for another deformed hypernucleus, $^{28}_{\Lambda}$Si, whose deformation can be roughly estimated as $\beta \approx 0.4$ [97,98,114] by the one of its adjacent isotope. With $\gamma = 0.4$, this value is also predicted theoretically, and the Λ $1s$ removal energy is $B_{\Lambda_s} = 16.7$ MeV, close to the experimental value 17.2 ± 0.2 MeV [96], while the theoretical and experimental removal energies for the $1p$ state are $B_{\Lambda_p} = 8.8$ and 7.6 ± 0.2 MeV, respectively. The effect of deformation on the splitting of the Λ $1p$ states is similar to that in $^{13}_{\Lambda}$C. With the same $a_4 = 3.15$ MeV fm^5, the predicted splitting between the [101 1/2] and [101 3/2] states is about 0.14 MeV, a little smaller than that in $^{13}_{\Lambda}$C, but there are currently no experimental data for this hypernucleus.

D. Structure of $^{89}_{\Lambda}$Y

Instead, results of a theoretical analysis of the (π^+, K^+) data for the hypernucleus $^{89}_{\Lambda}$Y are available, namely $E(1f_{5/2}) - E(1f_{7/2}) = 0.2 \pm 0.06$ MeV [21]. We therefore study this case in Fig. 7. This (hyper)nucleus is predicted to be undeformed or very slightly deformed when taking into account the intrinsic deformation of the Λ $1p$ orbits, cf. Fig. 6(a) at $\gamma = 1$ for $^{13}_{\Lambda}$C, while experimental data regarding deformation are not available. The SLL4 force reproduces nearly

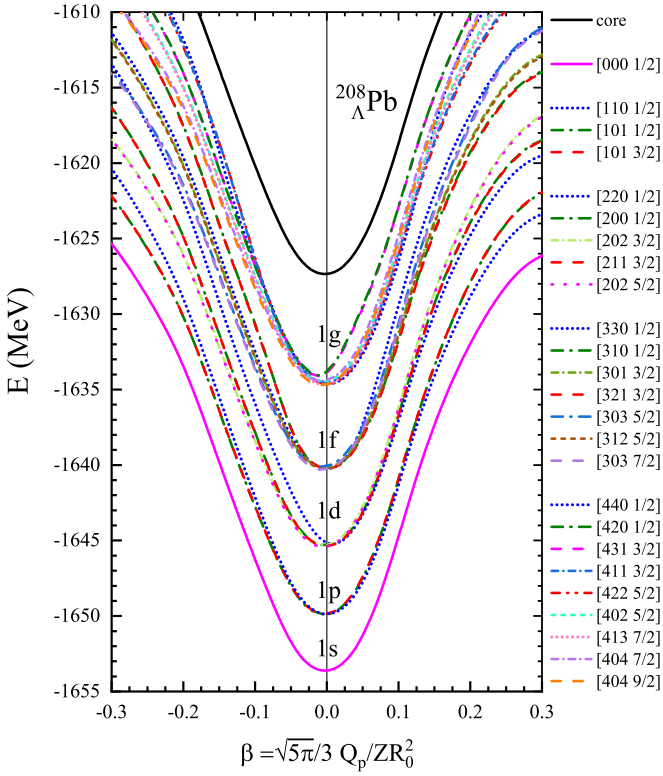

FIG. 9. Same as Fig. 7, for $^{208}_{\Lambda}$Pb.

perfectly the Λ s.p. levels in the spherical calculation, see Fig. 1. The Λ $1f$ level is split up into seven substates by s.o. force and deformation. The experimentally relevant splitting occurs between the [303 5/2] and [303 7/2] substates [21], and its value is reported in Fig. 8 as a function of a_4, together with all other splittings of the Λ $1p, d, f$ states. We note that the predicted $1f_{(5,7)/2}$ splitting with $a_4 = 3.15$ MeV fm^5 is about 0.4 MeV, somewhat higher than the value deduced from a distorted wave impulse approximation analysis of the ^{89}Y$(\pi^+, K^+)^{89}_{\Lambda}$Y reaction [21], which would correspond to $a_4 \approx 2$ MeV fm^5. But more detailed experimental data are required for a precise determination. In any case, this confirms that also in this hypernucleus the ΛN s.o. force is very small.

E. Spin symmetries in $^{208}_{\Lambda}$Pb

The same analysis is carried out for the heavy spherical hypernucleus $^{208}_{\Lambda}$Pb in Figs. 9 and 10, where the latter shows the splitting of the Λ $1s, p, d, f, g$ levels as a function of a_4 in comparison with the corresponding data [96]. With increasing a_4, the upper j levels gain binding energy, while the lower ones are less affected or decrease. The size of the splitting increases with l, consistent with the RMF calculations [29]. Values of $a_4 \gtrsim 10$ MeV fm^5 can be excluded by the current data.

We further visualize the splitting of SS for $^{208}_{\Lambda}$Pb in Fig. 11, namely the Λ removal energies of seven sets of spin doublets, $1p, d, f, g, h$ and $2p, d$. All spin doublets are found to be quasidegenerate. As observed in Fig. 10, for the same principal quantum number n, the splitting increases with orbital angular momentum l, as expected.

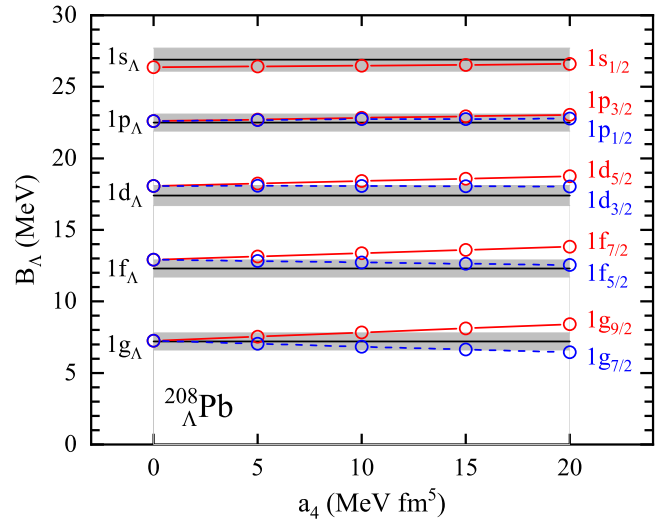

FIG. 10. The Λ removal energies B_Λ in $^{208}_{\Lambda}$Pb as functions of the ΛN s.o. force coupling strength a_4. The black lines denote the experimental data, and the gray bands the corresponding uncertainties [96].

Finally, in Fig. 12 the so-called reduced s.o. splittings

$$\Delta E_{\text{s.o.}} = (B_{\Lambda j_>} - B_{\Lambda j_<})/(2l+1) \tag{11}$$

are plotted versus the average Λ removal energies

$$E_{\text{av}} = (B_{\Lambda j_<} + B_{\Lambda j_>})/2 \tag{12}$$

for different values of a_4. For the orbits with the same principal quantum number, $\Delta E_{\text{s.o.}}$ exhibits a good linear correlation with E_{av}, for any fixed a_4. For $a_4 = 3.15$ MeV fm^5, the reduced splittings are less than 0.1 MeV for all spin doublets, which are much smaller than those in single-nucleon spectra.

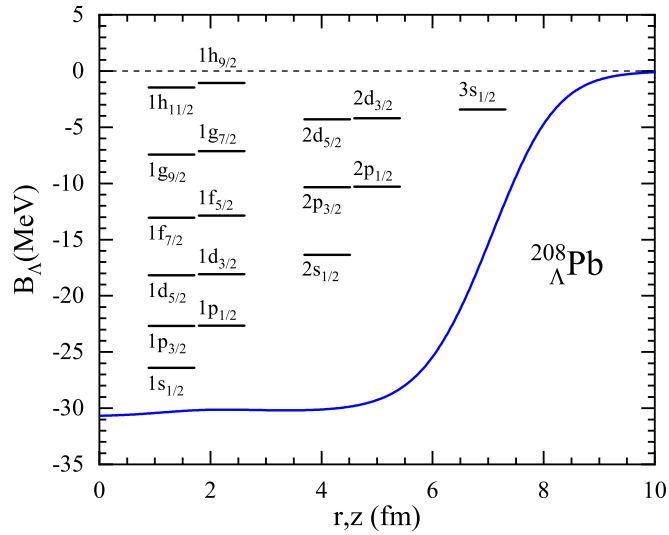

FIG. 11. Λ removal energies in $^{208}_{\Lambda}$Pb. The $n = 1, 2$ spin doublets obtained with $a_4 = 3.15$ MeV fm^5 are indicated. The corresponding $1s$ Λ potential is also shown.

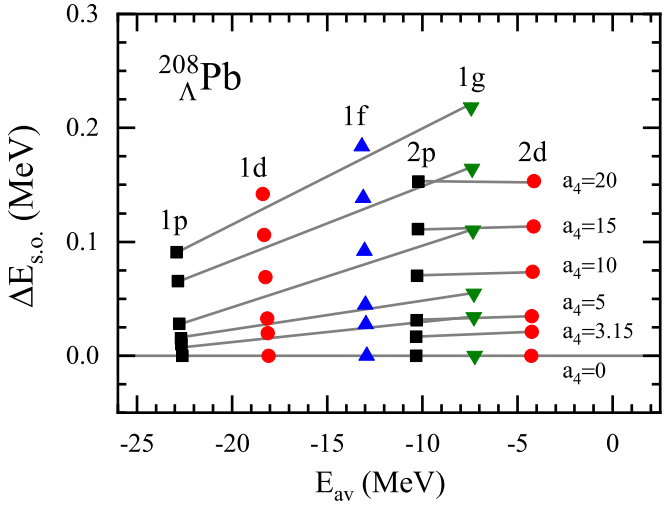

FIG. 12. Reduced s.o. splittings $\Delta E_{\text{s.o.}}$ in $^{208}_{\Lambda}$Pb versus their average removal energies E_{av}, see Eqs. (11),(12), for varying ΛN s.o. coupling strength a_4. The lines indicate the linear relations for the doublets with the same principal quantum number.

This can be understood as the s.o. interaction of the hyperon is about 20–30 times smaller than that of the nucleons.

The SHF results presented here are qualitatively similar to those of the RMF calculation [29]. However, more quantitative conclusions would require obtaining the Λ $n = 1, 2$ levels more accurately for several hypernuclei, which might be achieved in the future precision experiments scheduled at JLab [106].

IV. SUMMARY

The energy levels of the major Λ s.p. shells in hypernuclei ranging from light to heavy masses as well as the spin symmetry in the corresponding Λ spectrum were investigated in the framework of the DSHF approach with the SLL4 ΛN force fitted to the current global data set of Λ hypernuclei.

The interplay of s.o. interaction and deformation on the s.o. splitting of the Λ orbitals is studied in detail. The currently available data on $^{13}_{\Lambda}$C and $^{89}_{\Lambda}$Y indicate a very small effective Skyrme s.o. force, $a_4 \approx 3$ MeV fm^5, which however depends on the theoretical quadrupole deformation of the hypernucleus, which also affects the splitting of the levels. Larger deformation requires a larger intrinsic s.o. force.

As in many cases the deformation of core nuclei is unknown experimentally, this will remain a principle problem for a future simultaneous determination of the ΛN Skyrme parameters $a_{0,1,2,3,4,...}$ in a global approach by taking into account deformation. It also requires a beyond-mean-field approach [23,80,82] as a more realistic treatment to deal with deformation, in particular for weakly bound s.p. states.

For the spin doublets with the same main quantum number n, the s.o. splitting increases with orbital angular momentum l, such that $\Delta E_{\text{s.o.}}$ shows a good linear correlation with E_{av}, even for larger ΛN s.o. strengths a_4.

ACKNOWLEDGMENTS

This work was supported by the National Natural Science Foundation of China under Grants No. 12175071, No. 12205103, and No. 12275141.

[1] O. Haxel, J. H. D. Jensen, and H. E. Suess, Phys. Rev. **75**, 1766 (1949).
[2] M. G. Mayer, Phys. Rev. **75**, 1969 (1949).
[3] J. N. Ginocchio, Phys. Rep. **414**, 165 (2005).
[4] H. Liang, J. Meng, and S.-G. Zhou, Phys. Rep. **570**, 1 (2015).
[5] S.-G. Zhou, J. Meng, and P. Ring, Phys. Rev. Lett. **91**, 262501 (2003).
[6] R. Lisboa, M. Malheiro, P. Alberto, M. Fiolhais, and A. S. de Castro, Phys. Rev. C **81**, 064324 (2010).
[7] A. Bohr, I. Hamamoto, and B. R. Mottelson, Phys. Scr. **26**, 267 (1982).
[8] J. Dudek, W. Nazarewicz, Z. Szymanski, and G. A. Leander, Phys. Rev. Lett. **59**, 1405 (1987).
[9] W. Nazarewicz, P. J. Twin, P. Fallon, and J. D. Garrett, Phys. Rev. Lett. **64**, 1654 (1990).
[10] T. Byrski *et al.*, Phys. Rev. Lett. **64**, 1650 (1990).
[11] M. Danysz and J. Pniewski, Lond. Edinb. Dublin philos. mag. **44**, 348 (1953).
[12] J. Hao, T. T. S. Kuo, A. Reuber, K. Holinde, J. Speth, and D. J. Millener, Phys. Rev. Lett. **71**, 1498 (1993).
[13] M. Baldo, G. F. Burgio, and H.-J. Schulze, Phys. Rev. C **61**, 055801 (2000).
[14] F. Hofmann, C. M. Keil, and H. Lenske, Phys. Rev. C **64**, 025804 (2001).
[15] J. Schaffner-Bielich, Nucl. Phys. A **835**, 279 (2010).
[16] I. Vidaña, Nucl. Phys. A **914**, 367 (2013).
[17] L. Tolos and L. Fabbietti, Prog. Part. Nucl. Phys. **112**, 103770 (2020).
[18] G. Burgio, H.-J. Schulze, I. Vidaña, and J.-B. Wei, Prog. Part. Nucl. Phys. **120**, 103879 (2021).
[19] M. May *et al.*, Phys. Rev. Lett. **47**, 1106 (1981).
[20] S. Ajimura *et al.*, Phys. Rev. Lett. **86**, 4255 (2001).
[21] T. Motoba, D. E. Lanskoy, D. J. Millener, and Y. Yamamoto, Nucl. Phys. A **804**, 99 (2008).
[22] H.-J. Schulze and E. Hiyama, Phys. Rev. C **90**, 047301 (2014).
[23] W.-Y. Li, J.-W. Cui, and X.-R. Zhou, Phys. Rev. C **97**, 034302 (2018).
[24] H.-T. Xue, Q. B. Chen, X.-R. Zhou, Y. Y. Cheng, and H.-J. Schulze, Phys. Rev. C **106**, 044306 (2022).
[25] J. Cohen and H. J. Weber, Phys. Rev. C **44**, 1181 (1991).
[26] P. Alberto, R. Lisboa, M. Malheiro, and A. S. de Castro, Phys. Rev. C **71**, 034313 (2005).
[27] S. Y. Ding, Z. Qian, B. Y. Sun, and W. H. Long, Phys. Rev. C **106**, 054311 (2022).
[28] T. Motoba, Nucl. Phys. A **639**, 135c (1998).
[29] T.-T. Sun, W.-L. Lu, and S.-S. Zhang, Phys. Rev. C **96**, 044312 (2017).
[30] M. Rayet, Ann. Phys. **102**, 226 (1976).
[31] M. Rayet, Nucl. Phys. A **367**, 381 (1981).
[32] D. J. Millener, C. B. Dover, and A. Gal, Phys. Rev. C **38**, 2700 (1988).

[33] Y. Yamamoto, H. Bandõ, and J. Žofka, Prog. Theor. Phys. **80**, 757 (1988).
[34] F. Fernández, T. López-Arias, and C. Prieto, Z. Phys. A **334**, 349 (1989).
[35] Y. Yamamoto, T. Motoba, and T. A. Rijken, Prog. Theor. Phys. Suppl. **185**, 72 (2010).
[36] N. Guleria, S. K. Dhiman, and R. Shyam, Nucl. Phys. A **886**, 71 (2012).
[37] H.-J. Schulze, *AIP Conference Proceedings* (AIP Publishing, USA 2019), Vol. 2130, p. 020009.
[38] P. M. M. Maessen, T. A. Rijken, and J. J. de Swart, Phys. Rev. C **40**, 2226 (1989).
[39] T. A. Rijken, V. G. J. Stoks, and Y. Yamamoto, Phys. Rev. C **59**, 21 (1999).
[40] V. G. J. Stoks and T. A. Rijken, Phys. Rev. C **59**, 3009 (1999).
[41] X.-R. Zhou, H.-J. Schulze, H. Sagawa, C.-X. Wu, and E.-G. Zhao, Phys. Rev. C **76**, 034312 (2007).
[42] T. A. Rijken, M. M. Nagels, and Y. Yamamoto, Prog. Theor. Phys. Suppl. **185**, 14 (2010).
[43] T. Rijken, M. Nagels, and Y. Yamamoto, Nucl. Phys. A **835**, 160 (2010).
[44] Y. Yamamoto, E. Hiyama, and T. Rijken, Nucl. Phys. A **835**, 350 (2010).
[45] T. A. Rijken, M. M. Nagels, and Y. Yamamoto, Few-Body Syst. **54**, 801 (2013).
[46] M. M. Nagels, T. A. Rijken, and Y. Yamamoto, Phys. Rev. C **99**, 044003 (2019).
[47] M. M. Nagels, T. A. Rijken, and Y. Yamamoto, Phys. Rev. C **102**, 054003 (2020).
[48] Y. Sugahara and H. Toki, Prog. Theor. Phys. **92**, 803 (1994).
[49] J. Mareš and B. K. Jennings, Phys. Rev. C **49**, 2472 (1994).
[50] Z. Ma, J. Speth, S. Krewald, B. Chen, and A. Reuber, Nucl. Phys. A **608**, 305 (1996).
[51] Y. N. Wang and H. Shen, Phys. Rev. C **81**, 025801 (2010).
[52] Y. Tanimura and K. Hagino, Phys. Rev. C **85**, 014306 (2012).
[53] R. L. Xu, C. Wu, and Z. Z. Ren, J. Phys. G: Nucl. Part. Phys. **39**, 085107 (2012).
[54] X.-S. Wang, H.-Y. Sang, J.-H. Wang, and H.-F. Lv, Commun. Theor. Phys. **60**, 479 (2013).
[55] Y.-T. Rong, Z.-H. Tu, and S.-G. Zhou, Phys. Rev. C **104**, 054321 (2021).
[56] J. Haidenbauer, U. G. Meißner, and A. Nogga, Eur. Phys. J. A **56**, 91 (2020).
[57] J. Haidenbauer and I. Vidaña, Eur. Phys. J. A **56**, 55 (2020).
[58] J. Haidenbauer and U.-G. Meißner, EPJ Web Conf. **271**, 05001 (2022).
[59] H. Nemura, Y. Akaishi, and Y. Suzuki, Phys. Rev. Lett. **89**, 142504 (2002).
[60] H. Le, J. Haidenbauer, U. G. Meissner, and A. Nogga, Eur. Phys. J. A **56**, 301 (2020).
[61] E. Hiyama, M. Kamimura, T. Motoba, T. Yamada, and Y. Yamamoto, Prog. Theor. Phys. **97**, 881 (1997).
[62] E. Hiyama and T. Yamada, Prog. Part. Nucl. Phys. **63**, 339 (2009).
[63] M. Isaka, M. Kimura, A. Dote, and A. Ohnishi, Phys. Rev. C **83**, 044323 (2011).
[64] M. Isaka, K. Fukukawa, M. Kimura, E. Hiyama, H. Sagawa, and Y. Yamamoto, Phys. Rev. C **89**, 024310 (2014).
[65] M. Isaka and M. Kimura, Phys. Rev. C **92**, 044326 (2015).
[66] M. Isaka, Y. Yamamoto, and T. A. Rijken, Phys. Rev. C **94**, 044310 (2016).
[67] M. Isaka, Y. Yamamoto, and T. A. Rijken, Phys. Rev. C **95**, 044308 (2017).
[68] M. Isaka, Y. Yamamoto, and T. Motoba, Phys. Rev. C **101**, 024301 (2020).
[69] D. E. Lanskoy and Y. Yamamoto, Phys. Rev. C **55**, 2330 (1997).
[70] D. E. Lanskoy, Phys. Rev. C **58**, 3351 (1998).
[71] J. Cugnon, A. Lejeune, and H.-J. Schulze, Phys. Rev. C **62**, 064308 (2000).
[72] I. Vidaña, A. Polls, A. Ramos, and H.-J. Schulze, Phys. Rev. C **64**, 044301 (2001).
[73] H.-J. Schulze and T. Rijken, Phys. Rev. C **88**, 024322 (2013).
[74] P. Veselý, E. Hiyama, J. Hrtánková, and J. Mareš, Nucl. Phys. A **954**, 260 (2016).
[75] M. Fortin, S. S. Avancini, C. Providência, and I. Vidaña, Phys. Rev. C **95**, 065803 (2017).
[76] Y. Tanimura, Phys. Rev. C **99**, 034324 (2019).
[77] Y.-F. Chen, X.-R. Zhou, Q. Chen, and Y.-Y. Cheng, Eur. Phys. J. A **58**, 1 (2022).
[78] C. F. Chen, Q. B. Chen, X.-R. Zhou, Y. Y. Cheng, J.-W. Cui, and H.-J. Schulze, Chin. Phys. C **46**, 064109 (2022).
[79] J. Guo, C. F. Chen, X.-R. Zhou, Q. B. Chen, and H.-J. Schulze, Phys. Rev. C **105**, 034322 (2022).
[80] J. W. Cui, X. R. Zhou, and H.-J. Schulze, Phys. Rev. C **91**, 054306 (2015).
[81] H. Mei, K. Hagino, and J. M. Yao, Phys. Rev. C **93**, 011301(R) (2016).
[82] J.-W. Cui, X.-R. Zhou, L.-X. Guo, and H.-J. Schulze, Phys. Rev. C **95**, 024323 (2017).
[83] J.-W. Cui and X.-R. Zhou, Prog. Theor. Exp. Phys. **2017** 093D04 (2017).
[84] H. Mei, K. Hagino, J. M. Yao, and T. Motoba, Phys. Rev. C **97**, 064318 (2018).
[85] X.-R. Zhou, A. Polls, H.-J. Schulze, and I. Vidaña, Phys. Rev. C **78**, 054306 (2008).
[86] H.-J. Schulze, M. T. Win, K. Hagino, and H. Sagawa, Prog. Theor. Phys. **123**, 569 (2010).
[87] Y. Zhang, H. Sagawa, and E. Hiyama, Phys. Rev. C **103**, 034321 (2021).
[88] D. Vautherin, Phys. Rev. C **7**, 296 (1973).
[89] E. Chabanat, P. Bonche, P. Haensel, J. Meyer, and R. Schaeffer, Nucl. Phys. A **635**, 231 (1998).
[90] M. Bender, K. Rutz, P.-G. Reinhard, J. A. Maruhn, and W. Greiner, Phys. Rev. C **60**, 034304 (1999).
[91] N. Tajima, P. Bonche, H. Flocard, P.-H. Heenen, and M. Weiss, Nucl. Phys. A **551**, 434 (1993).
[92] T. Suzuki, H. Sagawa, and K. Hagino, Phys. Rev. C **68**, 014317 (2003).
[93] M. Bender, K. Rutz, P.-G. Reinhard, and J. Maruhn, Eur. Phys. J. A **8**, 59 (2000).
[94] P. Ring and P. Schuck, *The Nuclear Many Body Problem* (Springer Verlag, Berlin, 1980).
[95] M. T. Win, K. Hagino, and T. Koike, Phys. Rev. C **83**, 014301 (2011).
[96] A. Gal, E. V. Hungerford, and D. J. Millener, Rev. Mod. Phys. **88**, 035004 (2016).
[97] S. Raman, C. W. Nestor, and P. Tikkanen, At. Data Nucl. Data Tables **78**, 1 (2001).
[98] N. J. Stone, At. Data Nucl. Data Tables **111–112**, 1 (2016).

[99] O. Hashimoto and H. Tamura, Prog. Part. Nucl. Phys. **57**, 564 (2006).
[100] D. Davis, Nucl. Phys. A **754**, 3 (2005).
[101] M. Jurič *et al.*, Nucl. Phys. B **52**, 1 (1973).
[102] E. Botta, T. Bressani, and A. Feliciello, Nucl. Phys. A **960**, 165 (2017).
[103] M. Agnello *et al.*, Phys. Lett. B **622**, 35 (2005).
[104] M. Agnello *et al.*, Phys. Lett. B **698**, 219 (2011).
[105] M. T. Win and K. Hagino, Phys. Rev. C **78**, 054311 (2008).
[106] F. Garibaldi *et al.*, EPJ Web Conf. **271**, 01007 (2022).
[107] Q. N. Usmani and A. R. Bodmer, Phys. Rev. C **60**, 055215 (1999).
[108] E. Hiyama, M. Kamimura, K. Miyazaki, and T. Motoba, Phys. Rev. C **59**, 2351 (1999).
[109] K. Tanida *et al.*, Phys. Rev. Lett. **86**, 1982 (2001).
[110] B.-C. Fang, W.-Y. Li, C.-F. Chen, J.-W. Cui, X.-R. Zhou, and Y.-Y. Cheng, Eur. Phys. J. A **56**, 11 (2020).
[111] H. Kohri *et al.*, Phys. Rev. C **65**, 034607 (2002).
[112] H. Sagawa, X. R. Zhou, X. Z. Zhang, and T. Suzuki, Phys. Rev. C **70**, 054316 (2004).
[113] Y. Jin, X.-R. Zhou, Y.-Y. Cheng, and H.-J. Schulze, Eur. Phys. J. A **56**, 135 (2020).
[114] National Nuclear Data Center, https://www.nndc.bnl.gov/nudat3/.